ELSEVIER

Journal of Power Sources 87 (2000) 84–91

JOURNAL OF POWER SOURCES

www.elsevier.com/locate/jpowsour

# Pulverization and corrosion studies of bare and cobalt-encapsulated metal hydride electrodes

Anand Durairajan, Bala S. Haran, Ralph E. White, Branko N. Popov *

*Department of Chemical Engineering, University of South Carolina, Columbia, SC 29208, USA*

Received 24 July 1999; accepted 1 September 1999

**Abstract**

Electrochemical impedance spectroscopy was used as an in situ technique to determine the average particle size of metal hydride electrodes. Using this, the pulverization of bare and cobalt-encapsulated $LaNi_{4.27}Sn_{0.24}$ alloy was studied as a function of charge–discharge cycles. In the case of bare alloy, pulverization causes an exponential decay in particle size with cycling. Cobalt-encapsulated alloys do not undergo much pulverization with cycling. Bode responses obtained for bare alloy electrodes indicate the increase in particle to particle resistance with cycling. Alloy oxidation, which is responsible for the increase in particle to particle resistance is absent in the case of cobalt encapsulated alloy. Surface analysis indicates the presence of alloy segregation for bare $LaNi_{4.27}Sn_{0.24}$. Decrease in particle size and increase in bare alloy resistance is accompanied with severe decay in electrode discharge capacity. 

*Keywords:* Pulverization; Corrosion; Metal hydride electrodes

## 1. Introduction

Hydrogen storage alloys such as La–Ni, Mm (Misch metal)–Ni and Zr–Ni systems have received attention as a negative electrode material for rechargeable battery systems. These metal hydride alloys have a high energy density and are environmentally benign unlike the conventional Ni–Cd systems. However, the cycle lives of these alloys cause a great concern for use in practical Ni–MH batteries. Therefore, many researchers have focused on investigating the degradation mechanism of the metal hydride electrodes during charge–discharge cycling. Willems [1] explained that the decrease of the discharge capacity during cycling in La–Ni systems was due to the formation of $La(OH)_3$, which is not a hydrogen absorbing phase, at the surface. Sakai et al. [2] have cited the alloy pulverization and subsequent disintegration due to corrosion as important reasons for capacity fade of metal hydride alloys.

Surface segregation arises because any one element of the multi component alloy diffuses to the surface, due to its lower surface energy compared to other constituents. The element rapidly gets converted to oxides and hydroxides by bonding with the oxygen diffusing from positive electrode resulting in the decomposition of the alloy at the surface [3–5]. The volume expansion and contraction associated with the greater molar volume of hydrogen in the hydride phase leads to an internal stress in the alloy particle. The repeated adsorption/desorption of hydrogen during cycling results in pulverization of the alloy due to internal stress [6]. These pulverized alloy particles are exposed to the corroding electrolyte and are subjected to further segregation and degradation [7]. Further pulverization leads to loss of electrical contact between the alloy particles leading to an increase in particle–particle contact resistance thereby decreasing the charging efficiency. Though segregation and decomposition result in a small amount of loss of active material in a single charge–discharge cycle, their cumulative effects over hundreds of cycles result in a significant capacity loss for the electrode [8].

Hence, characterizing the extent of alloy pulverization and the alloy oxidation is very important for studying the performance of metal hydride alloys. Pulverization studies involve measuring changes in the alloy particle size during different cycles. Unfortunately, conventional methods for particle size measurements like SEM, TEM require break-

* Corresponding author. Tel.: +1-803-777-7314; fax: +1-803-777-8265; e-mail: popov@engr.sc.edu

0378-7753/00/$ - see front matter 
PII: S0378-7753(99)00399-7

ing of the battery for an image analysis of active material. These techniques, however accurate, still render the battery useless for further cycling. A novel imaging technique that will measure the particle size in-situ during cycling is needed. Further, alloy oxidation and segregation studies involve measuring the changes in particle to particle resistance during cycling and surface analysis.

Electrochemical impedance spectroscopy (EIS) has been used to characterize hydrogen diffusion in the particle [9,10]. Haran et al. [9] developed a first principles model for determining the hydrogen diffusion coefficient in metal hydrides by impedance spectroscopy. The model used the slope of transition diffusion regimes in Nyquist plots to calculate the diffusion coefficient. Our objective was to extend the model's applications to determine the average alloy particle size during cycling. This was used as an in-situ technique for characterizing the pulverization in an $AB_5$ type hydride namely, $LaNi_{4.27}Sn_{0.24}$. Further, the particle size calculated using the model would be verified with that found using other conventional methods. Bode plots obtained from EIS were used to obtain the particle to particle resistance during cycling. Electron probe microscopy analysis (EPMA) was used as a surface analysis technique to study the alloy segregation during cycling. Our previous studies indicate that cobalt microencapsulation improves the cycling performance of metal hydride alloys [11]. Hence, similar pulverization and alloy oxidation studies were performed on the cobalt encapsulated electrodes and the results obtained were compared with those obtained for the bare alloy.

## 2. Experimental

$LaNi_{4.27}Sn_{0.24}$ alloy was passed through various sieves after mechanical pulverization. The metal hydride powders were separated into 5 particle size fractions namely, (i) 15–25 μm, (ii) 53–63 μm, (iii) 63–75 μm, (iv) 90–106 μm and (v) $>250$ μm. Cobalt encapsulation was done using the method described in our earlier work [11]. Particle size was also calculated from BET surface area measurements and distribution plots were obtained using Laser particle size analyzers. Pellet electrodes were then prepared by mixing the alloy with 5% w/o PTFE binder followed by hot pressing this mixture between two-nickel meshes at 300°C and 6 ton/cm$^2$ in a cylindrical press. Characterization studies were done in a three-electrode setup. The working pellet electrode was inserted between two pieces of plexiglass and immersed in the cell filled with 6 M KOH solution. Hg/HgO was used as the reference electrode. The counter electrode was $Ni(OH)_2$/NiOOH. The cell was maintained at a constant temperature of 25°C using a water bath. Bitrode Model LCN automated cycle life tester was used for cycling the electrode. Electrochemical studies were done using the model 352 SoftCorr system with EG&G Princeton applied Model 273 potentiostat/galvanostat and a frequency analyzer. The electrodes were cycled at 0.1 C rate. The electrode was left on open circuit for 1 h after each discharge. After the potential stabilized, impedance studies were performed. The electrode was stable during the experiments and its open circuit potential changed less than 1 mV. The impedance data generally covered a frequency range of 1 mHz to 100 kHz. A sinusoidal ac voltage signal varying by $\pm 5$ mV was applied.

## 3. Impedance model

Haran et al. [9] developed a first principle analytical model for the impedance of spherical metal hydride particle. Since this is relevant to our studies, we present some salient features of this model. The electrode reaction at the surface of the hydride particle is,

$$MH_{x,ads} + xOH^- \underset{\text{charge}}{\overset{\text{discharge}}{\leftrightarrow}} M + xH_2O + xe^- \quad (1)$$

Since ohmic losses are neglected, the current at the interface due to reaction (1) depends on the hydrogen concentration at the surface, $c_s$ and also on the surface overpotential, $\eta_s$.

Assuming Fickian diffusion and solving the resulting partial differential equations we have the surface concentration as,

$$\bar{c}_s = \frac{c^o}{p} - \frac{\bar{j} w_{MH} R}{a_{MH} V(1-\varepsilon) F D} \frac{\sinh\left(\sqrt{\frac{pR^2}{D}}\right)}{\sqrt{\frac{pR^2}{D}}\cosh\left(\sqrt{\frac{pR^2}{D}}\right) - \sinh\left(\sqrt{\frac{pR^2}{D}}\right)} \quad (2)$$

where, the overbar indicates the Laplace domain. The faradaic impedance of this system in the frequency domain is obtained as,

$$Z(\omega) = \frac{\partial \bar{\eta}_s}{\partial \bar{j}} + \frac{(1-i)\sigma}{\sqrt{\omega}\left[\coth[(1+i)\psi] - \frac{(1-i)}{2\psi}\right]} \quad (3)$$

where $\sigma$ (Warburg coefficient) is given by

$$\sigma = \frac{\left(\partial \bar{j}/\partial \bar{c}_s\right)}{\left(\partial \bar{j}/\partial \bar{\eta}_s\right)}\left[\frac{w_{MH}}{a_{MH} V(1-\varepsilon) F\sqrt{2D}}\right] \quad (4)$$

and

$$\psi = \sqrt{\frac{\omega R^2}{2D}} \quad (5)$$

The first term in Eq. (3) corresponds to the faradaic impedance and the second term gives the diffusion

impedance. An important parameter in Eq. (5) is the time for diffusion ($t_D = R^2/D$), which controls the hydrogen transport rate in the alloy. Separating the diffusion impedance into real (Re) and imaginary (Im) parts we have,

$$Z(\omega) = \mathrm{Re} + i\,\mathrm{Im} \tag{6}$$

where

$$\mathrm{Re} = \frac{\sigma}{\sqrt{\omega}}\left[\frac{(T_1 - T_2)}{(T_1^2 + T_2^2)}\right] \tag{7}$$

$$\mathrm{Im} = -\frac{\sigma}{\sqrt{\omega}}\left[\frac{(T_1 + T_2)}{(T_1^2 + T_2^2)}\right] \tag{8}$$

$$T_1 = \frac{\sinh(\psi)\cosh(\psi)}{\sinh(\psi)^2 + \sin(\psi)^2} - \frac{1}{2\psi} \tag{9}$$

$$T_2 = -\frac{\sin(\psi)\cos(\psi)}{\sinh(\psi)^2 + \sin(\psi)^2} + \frac{1}{2\psi} \tag{10}$$

Differentiating the real part (given by Eq. (7)) and the imaginary part (given by Eq. (8)) we obtain the slope of the diffusion controlled impedance plot,

$$\frac{d(\mathrm{Im})}{d(\mathrm{Re})} = \frac{T_4[-T_3 + (S_3S_5 + S_4S_7 - S_1S_6 + S_2S_8)\psi] - 2T_3(S_4S_3 + S_2S_1)\psi}{T_4[-T_5 + (S_3S_6 + S_4S_8 - S_1S_5 + S_2S_7)\psi] - 2T_5(S_4S_3 + S_2S_1)\psi} \tag{11}$$

where

$$T_3 = (S_4S_5 - S_2S_6);\ T_4 = (S_4^2 + S_2^2);\ T_5 = (S_4S_6 + S_2S_5) \tag{12}$$

and

$$S_1 = S_5S_6;\ S_2 = 2\psi - S_5;$$

$$S_3 = 2\coth(\psi)\cot(\psi)(1 - \psi S_6) - 2\psi S_5 + S_8 \tag{13}$$

$$S_4 = 2\psi\coth(\psi)\cot(\psi) - S_6;\ S_5 = \coth(\psi) - \cot(\psi) \tag{14}$$

$$S_6 = \coth(\psi) + \cot(\psi);\ S_7 = 2 - S_1;$$

$$S_8 = \cot(\psi)^2 + \coth(\psi)^2 \tag{15}$$

Eq. (11) involves only the parameter $\psi$ (given by Eq. (5)) and can be used to extract the particle size by equating it to the slope in the transition region [12]. The model simulations and the diffusion coefficient calculations were done using Maple®.

## 4. Results and discussions

Hydrogen transport in a metal hydride particle has been shown to take place by a hopping mechanism. This hopping mechanism is simplified as a diffusion process with hydrogen diffusion coefficient and particle size of metal hydride alloy as the controlling parameters. Three-regions namely semi-infinite diffusion, transition and finite diffusion characterize the impedance response of a hydride electrode.

Fig. 1a shows a plot of the transition frequency vs. particle size. This frequency corresponds to the transition region before diffusion control dominates the impedance profile. Along with the diffusion coefficient, particle size determines the rate of hydrogen transport in the metal hydride alloy. During discharge hydrogen is consumed at the surface of the particle according to Eq. (1). This consumption creates a concentration gradient fueling further hydrogen transport from the interior to the alloy surface. In case of larger particles, it would take a longer time for hydrogen to diffuse through to the surface. This affects the transition from semi-infinite to complete diffusion control. As the frequency is inversely proportional to the time for diffusion ($t_D$), it is seen that the transition happens at lower frequency for larger particles. As the particle size decreases, the transition is shifted to higher

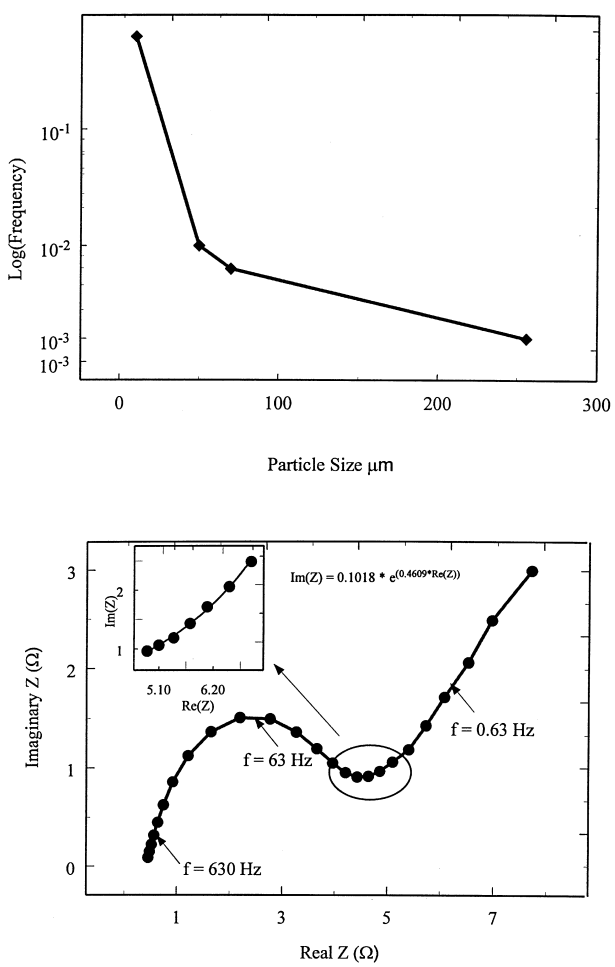


Fig. 1. A plot of transition frequency vs. particle size for $LaNi_{4.27}Sn_{0.24}$ alloy electrode (a). The data from the transition region is fitted exponentially to obtain the time for diffusion ($t_D$) and hence the particle size (b).

Table 1
Comparison of particle size obtained using impedance model and sieve analysis

| Particle size, μm (sieve analysis) | $D/R^2$, $s^{-1}$ (using model)[a] | Particle size, μm (using model) |
|---|---|---|
| 15–25 | 0.00511300 | 23.88 |
| 53–63 | 0.00059179 | 70.20 |
| 63–75 | 0.00042340 | 83.04 |
| 90–106 | 0.00029150 | 100 |
| >150 | 0.00011400 | 160 |

[a]A constant diffusion coefficient was used in all cases ($D = 0.73 \times 10^{-12}$ $cm^2/s$).

frequency values. Another way to look at this would be that diffusional limitations set in early for large particles.

In order to determine the particle size, the data from the transition region is fitted to an exponential equation. This is shown in Fig. 1b for a particle size of 90–106 μm. Differentiating the curve fit equation gives the slope of the transition regime. This slope is then equated to Eq. (11) and is solved for $\psi$. Knowing the value of the transition frequency, the ratio $D/R^2$ is found from Eq. (5). The particle size at a given cycle is calculated from this ratio with prior knowledge of the diffusion coefficient. These sets of calculations were done for three data points at the transition frequency and the average values were found. Initially, we found $D$ for a given particle size and used this value in subsequent calculations. Haran et al. [9] have shown that the diffusion coefficient of hydrogen in metal hydride electrodes is a function of depth of discharge (DOD). Since, we plan to compare the particle size change with cycling it is critical to collect impedance data at the same DOD. This has been achieved by doing impedance analysis after complete discharge of the pellet electrode, i.e., at 0% SOC for all cases.

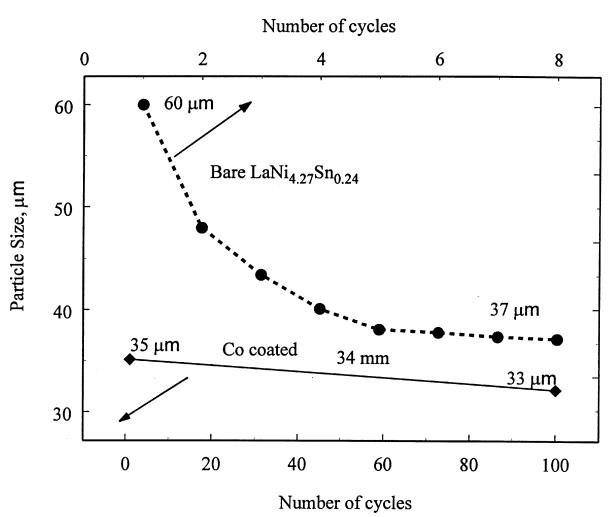


Fig. 2. Alloy pulverization in metal hydride electrode made of cobalt encapsulated and bare $LaNi_{4.27}Sn_{0.24}$. Particle size stabilizes after a few cycles at 38 μm in case of 53–63 μm size bare alloy electrode. Cobalt-coated electrode do not pulverize significantly during cycling.

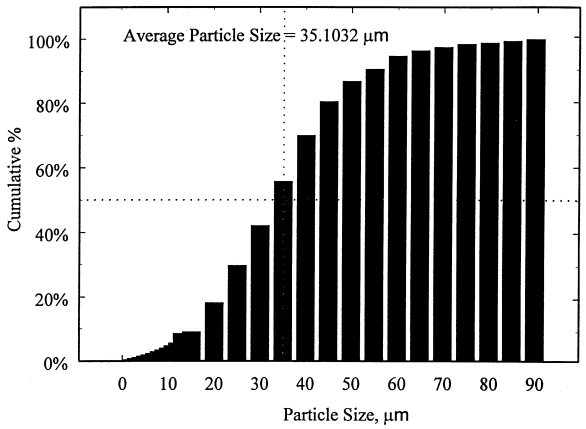


Fig. 3. Initial particle size distribution of cobalt-encapsulated electrode obtained using Laser Sieve analysis.

Table 1 presents the $D/R^2$ and hence particle diameter ($2R$) calculated from Nyquist plots of $LaNi_{4.27}Sn_{0.24}$ alloy of different sizes. These measurements were carried out after the very first discharge and hence the particle size is very close to the initial value obtained by sieve analysis. Good agreement is seen between the model calculation and actual data. Particle size reduction during cycling determines the performance of metal hydride alloys. The next set of studies show the pulverization behavior of $LaNi_{4.27}Sn_{0.24}$ alloy for a given particle size namely, 53–63 μm.

Fig. 2 shows the particle size reduction with cycling in case of $LaNi_{4.27}Sn_{0.24}$ alloy. Pulverization behavior of cobalt encapsulated $LaNi_{4.27}Sn_{0.24}$ alloy is also presented. Particle size was measured at the end of each discharge cycle using impedance analysis. It is seen that the pulverization is very large initially and follows an exponential decrease with cycling. Volume expansion due to the hydrogen absorption leads to breaking of the alloy particles. Initially, for the 53–63 μm particle, the surface area is

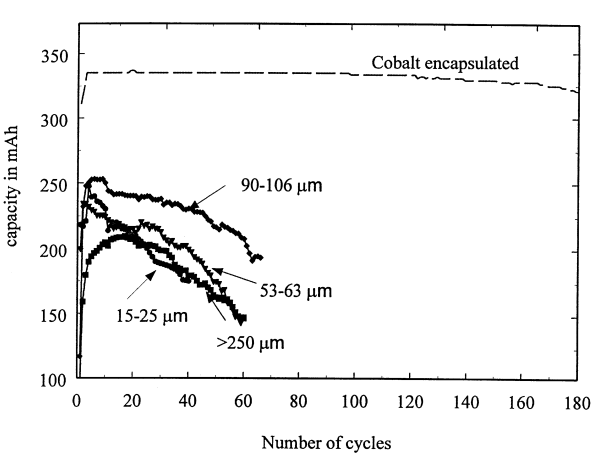


Fig. 4. Cycle life studies on $LaNi_{4.27}Sn_{0.24}$ alloy electrodes of different particle sizes. Capacity fade behavior of cobalt encapsulated electrode is shown for comparison.

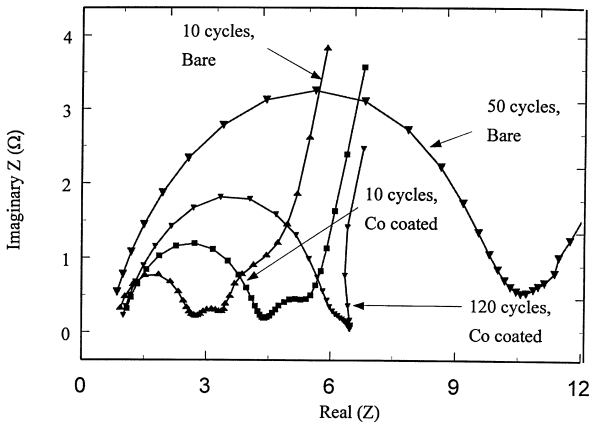


Fig. 5. Nyquist plot of the impedance response of bare and cobalt coated $LaNi_{4.27}Sn_{0.24}$ at different cycles.

small (0.02774 $m^2/g$ calculated using BET) and hence the stress acting on it is very high. But as the particle continually breaks, the stress acting on the broken particle gradually decreases and the pulverization becomes less. It is seen that the particle size stabilizes after few cycles at 38 μm. However, this pulverization behavior is specific for the alloy taken for study and would vary depending on the volume expansion of the alloy. The broken particles undergo less pulverization, but they offer a large area for corrosion to occur. This results in oxidation of the alloy to inactive material and hence lower capacity and faster corrosion.

Cobalt encapsulated alloy on the other hand does not show much pulverization. The initial particle size found using laser sieve analysis is shown in Fig. 3. Pulverization studies done in a similar way indicate that there is not much change in the particle size with cycling. The particle size decreased from 35 μm initially to 33 μm after 120 cycles. Lesser pulverization would also mean lesser corrosion and better particle to particle contact. This results in a longer cycle life and lesser capacity fade. The corrosion and capacity fade of cobalt encapsulated and bare $LaNi_{4.27}Sn_{0.24}$ alloy of different sizes was studied next.

Fig. 4 shows the cycle life studies done on $LaNi_{4.27}Sn_{0.24}$ electrode for four different particle sizes. Cycle life of cobalt encapsulated alloy is shown for comparison. Even though the pulverization had subsided after 8 cycles (from Fig. 2), the capacity fade continues to be there. This can be understood from the fact that apart from pulverization, alloy corrosion also influences the capacity in metal hydride alloys. Alloy oxidation is believed to be one of the most important reasons for capacity decay. Oxidation of lanthanum to lanthanum oxides has been found to be an important cause of capacity decay. Studies have shown the diffusion of fresh lanthanum to the surface from the bulk, where it gets oxidized. Lanthanum oxidation and segregation results in the decrease of the dehydriding capacity of the electrode.

It is seen that electrodes made of smaller particles (15–25 μm) undergo a severe capacity decay compared to those made of bigger particles (53–63 μm and 90–106 μm). This is due to the much larger surface area of the smaller particles as compared to the bigger ones. Similar results have also been seen by Sako et al. in their study on $MmNi_{3.5}Al_{0.3}Co_{0.8}Mn_{0.4}$ alloy of different sizes [13]. An optimum size exists, above and below which the capacity fade is severe. It is evident that electrode packing and design play a crucial role in optimizing alloy performance. Cobalt encapsulated alloy has a cycle life of more than 180 cycles. Cobalt encapsulation forms a protective cover over the alloy surface and prevents it from oxidation. The absence of protective cover in bare alloy is reflected in the capacity decay of the electrodes.

EIS under zero current conditions enables the determination of the oxidation resistance and evaluation of alloy corrosion [14] without the interference of any of the ohmic resistances (related to alloy particle contact resistance and electrolyte resistance). According to Kuriyama et al. [15,16], the total resistance of the system is a sum of the following resistances: (i) the electrolyte resistance, (ii) the resistance between the current collector and the electrode pellet, (iii) the alloy particle to particle contact resistance and (iv) the polarization resistance which is related to the electrode reaction on the alloy surface and is inversely proportional to the active surface area. Fig. 5 shows the impedance response for bare (initial particle size 53–63 μm) and cobalt coated $LaNi_{4.27}Sn_{0.24}$ electrode. The equivalent circuit used to determine the various resistances is given in Fig. 6. The parameter of interest namely the alloy resistance at the electrode/electrolyte interface was evaluated using this circuit. Initially, for both the bare alloy and Co coated electrode, two semi-circles are seen in the Nyquist plot. However, after 50 cycles for the bare

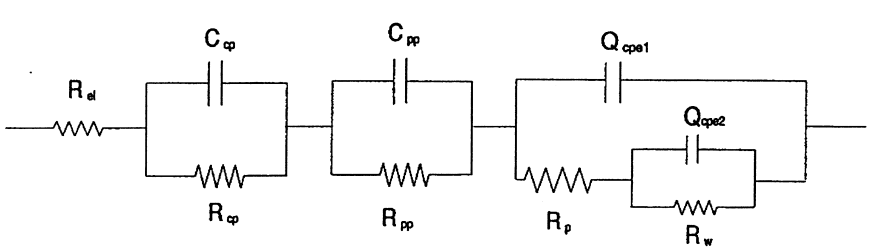


Fig. 6. Schematic of the equivalent circuit for the metal hydride electrode.

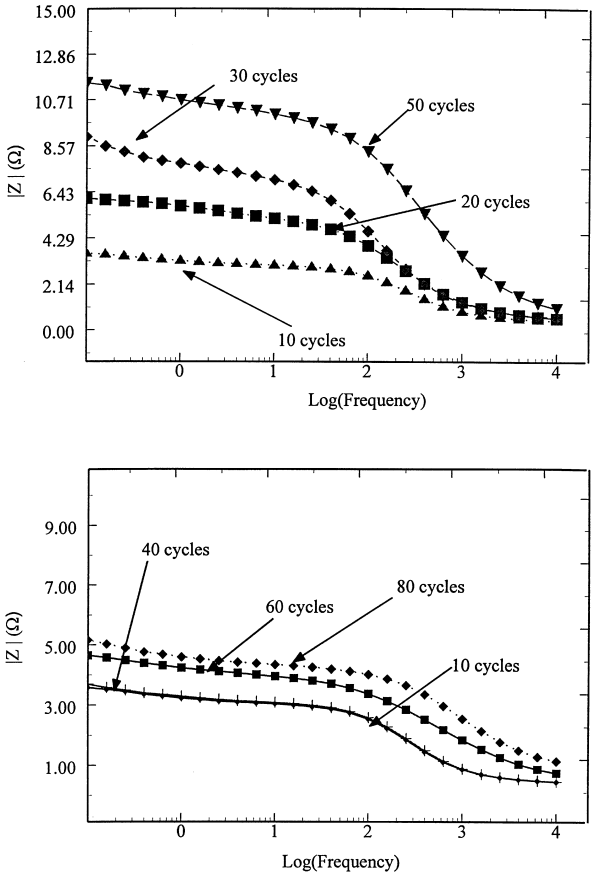


Fig. 7. Bode plot of impedance response in $LaNi_{4.27}Sn_{0.24}$ alloy electrodes at different cycles. (a) Bare alloy (b) Cobalt-microencapsulated alloy.

alloy both semi-circles merge and significant increase in the alloy resistance is seen. The increase in resistance for the Co plated alloy is comparatively less even after 120 cycles.

The change in the bare alloy resistance with cycling is shown in Fig. 7a. Bode plots shown in Fig. 7a for the bare alloy reveal that the electrode resistance increases continuously during cycling. This is caused due to the formation of oxidized species at the alloy surface. These oxides do not hydride and further are highly resistive as evidenced by the increased impedance seen in Fig. 7a. Similar Bode plots for cobalt encapsulated electrode show a relatively constant alloy resistance (Fig. 7b) with cycling. The bene-

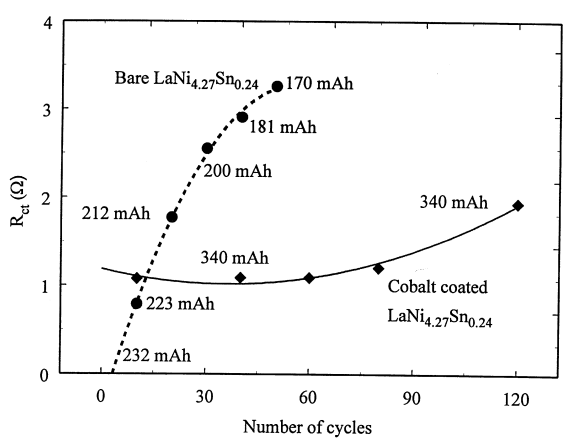


Fig. 8. Change of resistance with cycling for bare (53–63 μm) and cobalt coated $LaNi_{4.27}Sn_{0.24}$ electrodes with cycling. The resistance was obtained from impedance data.

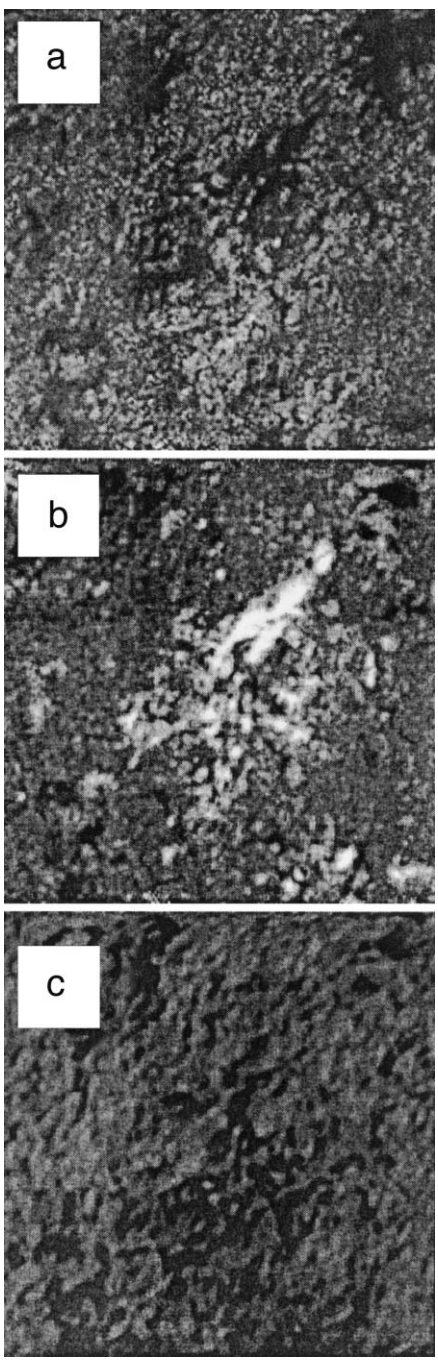


Fig. 9. EPMA of cycled $LaNi_{4.27}Sn_{0.24}$ alloy electrode. The recorded X-ray intensities are compared with standard intensities of Ni (a), La (b) and $O_2$ (c). Lanthanum- and oxygen-rich phases suggest alloy segregation.

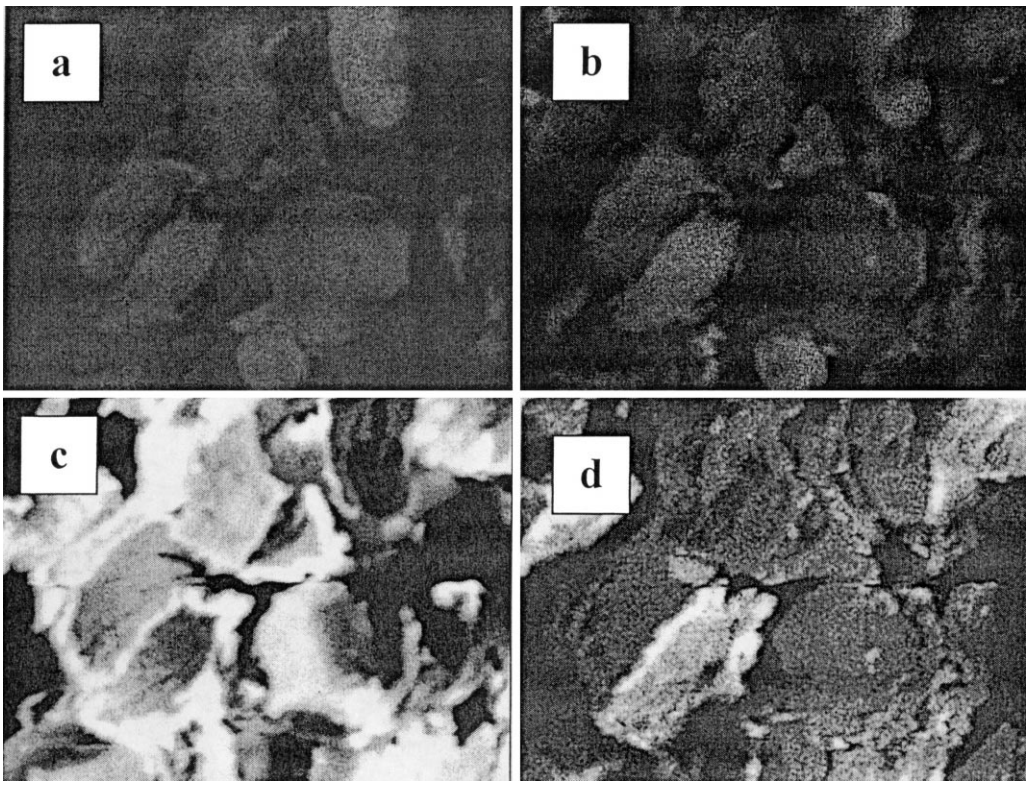


Fig. 10. EPMA of cycled cobalt coated $LaNi_{4.27}Sn_{0.24}$ alloy. The recorded X-ray intensities are compared with standard intensities of Ni (a), La (b) Co (c) and $O_2$ (d). Cobalt hydroxide present on the alloy surface protects the alloy from corrosion.

ficial cobalt cover protects the alloy from oxidation and also ensures electrical contact between the particles.

Fig. 8 presents the change in alloy resistance of the $LaNi_{4.27}Sn_{0.24}$ electrode (53–63 μm) and cobalt coated alloy with cycling. It is clearly seen that the bare alloy resistance increases due to oxide formation. Further, the oxides formed do not hydride and hence the capacity in subsequent cycles is significantly lower. These results agree with the capacity fade seen in Fig. 4. Cobalt coated alloy on the other hand cycles without any capacity fade and this is well explained by the constant alloy resistance as seen in Fig. 7b.

Fig. 9 is an EPMA of a cycled metal hydride negative electrode made of 90–106 μm (initial particle size) $LaNi_{4.27}Sn_{0.24}$ alloy. The recorded intensities of the X-ray map has been compared to the standard intensities of lanthanum, oxygen and nickel by way of color maps. The color maps uses a scale that corresponds to a black body radiation, with concentration equated to the temperature. Thus, the concentration of a particular species is high if the intensity map for that species is characterized by lot of white (bright) regions [17]. The high concentration of lanthanum oxides suggests the oxidation of active material with cycling. This segregation of specific alloy elements arises because any one element of the multicomponent alloy diffuses to the surface, due to its lower surface energy compared to the other constituents. In this case, since the surface energy of lanthanum is lower than that of nickel the surface becomes lanthanum enriched. This element rapidly gets converted to oxides and hydroxides by bonding with oxygen resulting in decomposition of alloy at the surface. Formation of oxides results in increasing the resistance of the alloy material.

Lanthanum oxides are considerably absent in case of cobalt encapsulated alloys. Fig. 10 shows the X-ray map of cycled electrode made of cobalt encapsulated $LaNi_{4.27}Sn_{0.24}$ alloy compared for standard intensities of nickel (a), lanthanum (b), cobalt (c) and oxygen (d). Cobalt and oxygen-rich phases confirm the presence of cobalt oxides on the alloy. It is seen that cobalt oxides that are present on the surface of the alloy protect it from oxidation.

## 5. Conclusions

Impedance responses of $LaNi_{4.27}Sn_{0.24}$ electrodes were obtained in the frequency range of 1 mHz to 100 kHz. The slopes of the transition region in the impedance profile were used to calculate the particle size of the alloy. Pulverization behavior for bare and cobalt coated $LaNi_{4.27}Sn_{0.24}$ alloy was studied by determining the parti-

cle size at the end of each discharge cycle. It is seen that the pulverization is more initially and it gradually slows down in an exponential way in case of bare alloy. Pulverization is seen to be insignificant in case of cobalt encapsulated alloy. Impedance spectroscopy as detailed in this work could be used as an in situ technique for determination of average particle size during cycling in metal hydride batteries. Cycle life studies on $LaNi_{4.27}Sn_{0.24}$ alloy show capacity decay even after the particle size stabilization. This shows that pulverization is not the only reason for capacity decay. Bode responses obtained for bare and cobalt plated alloy at different cycles show the presence of alloy oxidation in case of bare alloy. The particle to particle resistance increased significantly with cycling while the phenomena was minimum in case of cobalt coated alloy. X-ray maps show the presence of large amount of lanthanum oxides in the cycled bare alloy. This suggests that alloy oxidation is an important factor in the capacity fade of metal hydrides. Segregation was found to be a minimum in case of cobalt-plated alloy.

## Acknowledgements

Financial support by the Exploratory Technology Research (ETR) program, which is supported by the Office of Transportation Technologies (OTT) of the US Department of Energy (DOE), subcontract no. 4614610, is gratefully acknowledged.

## References

[1] J.J.J. Willems, Philips J. Res. 39 (1984) 1.
[2] T. Sakai, A. Yuasa, H. Ishikawa, H. Miyamura, N. Kuriyama, J. Less-Common Met. 172 (1991) 1175.
[3] T.L. Markin, R.M. Dell, J. Electroanal. Chem. 118 (1981) 217.
[4] L. Schlapbach, A. Seiler, H.C. Siegmann, T.V. Waldkrich, P. Zurcher, Int. J. Hydrogen Energy 4 (1979) 21.
[5] Y.Q. Lei, Z.P. Li, C.P. Chen, J. Wu, Q.D. Wang, J. Less-Common Met. 172 (1991) 1265.
[6] J.J.G. Willems, K.H. Buschow, J. Less-Common Met. 129 (1987) 13.
[7] L. Schlapbach, A. Seiler, F. Stucki, H.C. Siegmann, Int. J. Less-Common Met. 4 (1979) 21.
[8] T. Sakai, H. Ishikawa, H. Yoshinaga, K. Oguro, C. Iwakura, Prog. Batteries Sol. Cells 6 (1987) 221.
[9] B.S. Haran, B.N. Popov, R.E. White, J. Power Sources 75 (1998) 56.
[10] L.O. Valoen, S. Sunde, R. Tunold, J. Alloys Compd. 253 (1997) 656.
[11] A. Durairajan, B.S. Haran, B.N. Popov, R.E. White, Accepted for publication J. Power Sources, March 1999.
[12] S. Motupally, C.C. Streinz, J.W. Weidner, J. Electrochem. Soc. 142 (1995) 1401.
[13] Y. Sato, A. Togami, K. Ogino, N. Ishii, Denki Kagaku 12 (1993) 1429.
[14] G. Zheng, B.N. Popov, R.E. White, J. Electrochem. Soc. 143 (1996) 435.
[15] N. Kuriyama, T. Sakai, H. Miyamura, I. Uehara, H. Ishikawa, J. Alloys Compd. 202 (1993) 183.
[16] N. Kuriyama, T. Sakai, H. Miyamura, I. Uehara, H. Ishikawa, J. Alloys Compd. 192 (1993) 161.
[17] S.J.B. Reed, Electron Microprobe Analysis and Scanning Electron Microscopy in Geology, Cambridge Univ. Press, Cambridge, 96, 1993.